Surface Quasi-Conformal Mapping by Solving Beltrami Equations

W. Zeng[1], F. Luo[2], S.-T. Yau[3], and X.D. Gu[1]

[1] Computer Science Department, State University of New York at Stony Brook, USA
[2] Mathematics Department, Rutgers University, USA
[3] Mathematics Department, Harvard University, USA

Abstract. We consider the problem of constructing quasi-conformal mappings between surfaces by solving Beltrami equations. This is of great importance for shape registration.

In the physical world, most surface deformations can be rigorously modeled as quasi-conformal maps. The local deformation is characterized by a complex-value function, *Beltrami coefficient*, which describes the deviation from conformality of the deformation at each point.

We propose an effective algorithm to solve the quasi-conformal map from the Beltrami coefficient. The major strategy is to deform the conformal structure of the original surface to a new conformal structure by the Beltrami coefficient, such that the quasi-conformal map becomes a conformal map. By using holomorphic differential forms, conformal maps under the new conformal structure are calculated, which are the desired quasi-conformal maps.

The efficiency and efficacy of the algorithms are demonstrated by experimental results. Furthermore, the algorithms are robust for surfaces scanned from real life, and general for surfaces with different topologies.

Keywords: Quasic-Conformal Map, Beltrami Equation, Riemannian Metric, Uniformization.

1 Introduction

Computing the mappings between surfaces is of fundamental importance in many fields in science and engineering. Mappings will introduce distortions on surfaces, which can be measured by area distortion and angle distortion. Mappings without area or angle distortions are isometric, those without angle distortions are conformal. Isometric and conformal mappings are extremely rare in reality. Most mappings in the physical world have bounded angle distortion, which can be categorized as quasi-conformal mappings. Conformal mappings are fully determined by boundary conditions. Quasi-conformal mappings are determined by both boundary conditions and a function, the so-called Beltrami coefficient, defined on the source surface, therefore it gives point-wise control to the users. The detailed control of the mapping is crucial for many practical applications. This work focuses on how to construct quasi-conformal mappings from the given

E.R. Hancock et al. (Eds.): Mathematics of Surfaces 2009, LNCS 5654, pp. 391–408, 2009.

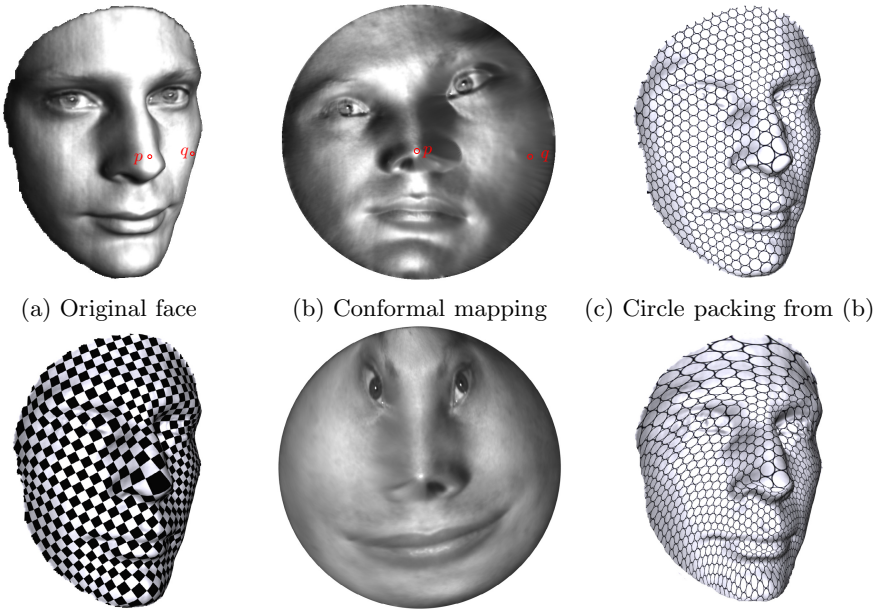

(a) Original face (b) Conformal mapping (c) Circle packing from (b)

(d) Checker-board texture (e) Quasi-conformal mapping (f) Circle packing from (e)

Fig. 1. Conformal and Quasi-Conformal mappings for a topological disk

Beltrami coefficients. Although the discussions are mainly on genus zero surfaces with an arbitrary number of boundaries, the method can be directly applied to surfaces with general topologies.

Suppose two surfaces S_1, S_2 have Riemannian metrics $\mathbf{g}_1$ and $\mathbf{g}_2$. A homeomorphism ϕ maps S_1 to S_2. We say ϕ is conformal, if it is angle-preserving. Mathematically, the pull back metric $\phi^*\mathbf{g}_2 = e^{2u}\mathbf{g}_1$. Locally, conformal mapping is just scaling, therefore the local shapes are well preserved. Figure 1 shows a conformal map from a human face surface (a) to the planar disk (b). From the planar image (b), it is obvious that the major facial features are well preserved. If we put a checker-board on the disk, and pull back the texture onto the face surface, all the right-angled corners of checkers are preserved (d). Geometrically, a conformal mapping maps infinitesimal circles to infinitesimal circles. As shown in the figure, the regular circle packing on the texture is pulled back to the face, and the shape of the circles is well preserved as shown in (c).

In general, conformal mappings are rare. Most mappings in physical world are quasi-conformal. Conformal mappings have no angle distortions, while quasi-conformal mappings introduce bounded angle distortion. Geometrically, a quasi-conformal map transforms infinitesimal circles on the source surface to infinitesimal ellipses on the target surface with bounded eccentricity. Figure 1(e) shows a quasi-conformal map from the face surface to the unit disk. Frames (c) and (f) show that the circles on the texture are mapped to the ellipses.

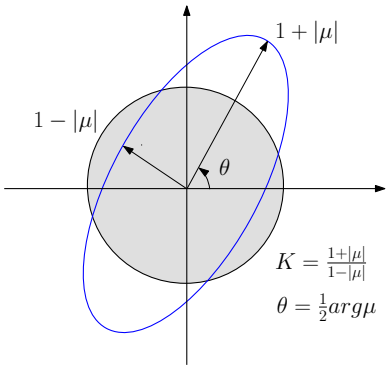

Fig. 2. Illustration of how Beltrami coefficient μ measures the distortion by a quasi-conformal mapping that maps a small circle to an ellipse with dilatation K

Quasi-conformal maps are controlled by both boundary condition and the so-called Beltrami coefficient μ. The characteristics of the infinitesimal ellipses, the orientation of the axis and the ratio between the longer axis and shorter axis are encoded in μ, but the scale factor is absent. In detail, let $\phi : S_1 \to S_2$ be the map, z and w local conformal parameters of $(S_1, \mathbf{g}_1)$ and $(S_2, \mathbf{g}_2)$, such that $\mathbf{g}_1 = e^{2u_1} dz d\bar{z}$, $\mathbf{g}_2 = e^{2u_2} dw d\bar{w}$, then ϕ has a local representation. The Beltrami coefficient is defined as

$$\frac{\partial \phi}{\partial \bar{z}} = \mu(z) \frac{\partial \phi}{\partial z}. \tag{1}$$

The ratio between the two axis of the ellipse is given by $K = \frac{1+|\mu(z)|}{1-|\mu(z)|}$ and the orientation of the axis is related to $arg\mu(z)$. As shown in Figure 2, two orthogonal lines associated with the circle are the principal distortion directions and the angle is measured between corresponding principal distortion directions.

The fundamental problem is to find a quasi-conformal map ϕ, which satisfies the given Beltrami coefficient μ, namely, solving Beltrami equations (see Eqn. 1). The major strategy is as follows. First, we compute conformal maps, $\phi_1 : S_1 \to \mathbb{D}_1$, $\phi_2 : S_2 \to \mathbb{D}_2$, where $\mathbb{D}_1$ and $\mathbb{D}_2$ are domains on the complex plane, with the canonical Euclidean metric $\mathbf{g}_0 = dz d\bar{z}$. Then we construct a quasi-conformal map $\tau : (\mathbb{D}_1, \mathbf{g}_0) \to (\mathbb{D}_2, \mathbf{g}_0)$, such that the Beltrami coefficient of τ equals to μ. Then the pullback metric on $\mathbb{D}_1$ induced by τ is

$$\tau^*(\mathbf{g}_0) = |\frac{\partial \tau}{\partial z}|^2 |dz + \mu d\bar{z}|^2,$$

which is conformal to the metric $\mathbf{g}_1 = |dz + \mu d\bar{z}|^2$, and then $\tau : (\mathbb{D}_1, \mathbf{g}_1) \to (\mathbb{D}_2, \mathbf{g}_0)$ is a conformal map. By changing the metric on $\mathbb{D}_1$ from $\mathbf{g}_0$ to $\mathbf{g}_1$, the quasi-conformal map τ becomes conformal and can be computed by using mature methods for conformal mappings, such as using Gu-Yau's method based on holomorphic differential forms. Finally, the desired quasi-conformal mapping satisfying the Beltrami equation (see Eqn. 1) is given by $\phi = \phi_2^{-1} \circ \tau \circ \phi_1$.

Figure 1 (e) and (f) show a quasi-conformal map, whose Beltrami coefficient is given by $\mu(z) = z$, where z is the conformal parameter as shown in (b). Near the nose tip, $\mu(z)$ is close to zero, therefore, the mapping there is close to be conformal, and the ellipses are rounder as illustrated in (f).

The paper is organized in the following way: Section 2 briefly review the most related works in the field; Section 3 introduces the theoretic background; Section 4 focuses on the computational methodologies; Section 5 reports the experimental results; the paper is concluded in Section 6.

2 Previous Work

Recently, with the development of digital scanning technology, computing conformal mappings between surfaces becomes more and more important. In computer graphics and discrete mathematics, much sound research has focused on discrete conformal mappings.

The computational method of current work is mainly based on harmonic maps and holomorphic differential forms. Here, we briefly overview most related work, and refer readers to [1, 2] for thorough surveys. For example, curvature flow is another important method for computing conformal mappings. In current work, we skip the curvature flow methods, such as discrete Ricci flow [3, 4].

Discrete harmonic maps were constructed in [5], where the cotan formula was introduced. First order finite element approximations of the Cauchy-Riemann equations were introduced by Levy et al. [6]. Discrete intrinsic parameterization by minimizing Dirichlet energy was introduced by [7]. Mean value coordinates were introduced in [8] to compute generalized harmonic maps; Discrete spherical conformal mappings were used in [9] and [10].

Discrete holomorphic forms were introduced by Gu and Yau [11] to compute global conformal surface parameterizations for high genus surfaces. Another approach of discrete holomorphy was introduced in [12] using discrete exterior calculus [13]. The problem of computing optimal holomorphic 1-forms to reduce area distortion was considered in [14]. Gortler et al. [15] generalized 1-forms to the discrete case, using them to parameterize genus one meshes. Tong et al. [16] generalized the 1-form method to incorporate cone singularities. Discrete one-forms have been applied for meshing point clouds in [17], surface tiling [18], surface quadrangulation [19]. The holomorphic 1-form method has been applied in virtual colonoscopy [20]. The colon surface is reconstructed from MRI images, and conformally mapped to the planar rectangle. This improves the efficiency and accuracy for detecting polyps. Conformal mapping is used for brain cortex surface morphology study in [10]. By mapping brain surfaces to spheres, cortex surface registration and comparison become straightforward. Holomorphic 1-form method has also been applied in computer vision [21, 22] for 3D shape matching, recognition and stitching. In geometric modeling field, constructing splines on general surfaces is one of the most fundamental problems. It is proven in [23] that if the surface has an affine structure, then splines can be generalized to it directly. Holomorphic 1-forms can be applied for computing the affine structures of general surfaces.

3 Theoretical Background

In this section, we briefly introduce the major concepts in differential geometry and Riemann surface theory, which are necessary to explain the quasi-conformal maps. We refer readers to [24, 25] for detailed information.

3.1 Conformal Structure and Riemann Surface

A Riemann surface is a surface with a complex structure, such that complex analysis can be defined on the surface.

Suppose $f : \mathbb{C} \to \mathbb{C}$ is a complex function. $f(x, y) = (u(x, y), v(x, y))$, f is *holomorphic*, if it satisfies the following *Cauchy-Riemann equations*,

$$\begin{cases} \frac{\partial u}{\partial x} = & \frac{\partial v}{\partial y} \\ \frac{\partial u}{\partial y} = & -\frac{\partial v}{\partial x} \end{cases}$$

If a holomorphic function f is a bijection, and the inverse f^{-1} is also holomorphic, then f is *biholomorphic*.

As shown in Fig.3, suppose S is a surface covered by a collection of open sets $\{U_\alpha\}$, $S \subset \bigcup_\alpha U_\alpha$. A chart is (U_α, ϕ_α), where $\phi_\alpha : U_\alpha \to \mathbb{C}$ is a homeomorphism. The chart transition function $\phi_{\alpha\beta} : \phi_\alpha(U_\alpha \cap U_\beta) \to \phi_\beta(U_\alpha \cap U_\beta)$, $\phi_{\alpha\beta} = \phi_\beta \circ \phi_\alpha^{-1}$. The collection of the charts $\mathcal{A} = \{(U_\alpha, \phi_\alpha)\}$ is called the *atlas* of S. If all chart transition functions are biholomorphic, then the atlas is called a *conformal atlas* of the surface. Two conformal atlases are compatible, if their union is still a conformal atlas. The union of all compatible conformal atlases is called the *conformal structure* of the surface. A surface with a conformal structure is called a *Riemann surface*.

Suppose S has a Riemannian metric $\mathbf{g}$, the local coordinates z_α is called *isothermal*, if the metric has local representation

$$\mathbf{g} = e^{2\lambda(z)} dz d\bar{z}.$$

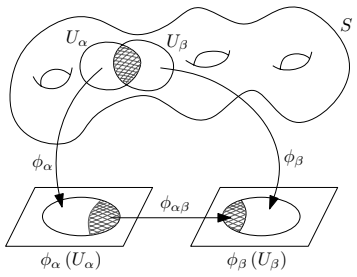

Fig. 3. A surface is covered by an atlas. If all chart transitions are holomorphic, the atlas is a conformal atlas. If all local coordinates are isothermal, the surface is a Riemann surface.

A conformal structure is compatible with the Riemannian metric, if all its local coordinates are isothermal. In practice, the surfaces of interest are embedded in $\mathbb{R}^3$, therefore with the induced Euclidean metric. The conformal structure compatible to the induced metric is our major focus.

Suppose ω is a complex differential form, such that on each chart (U_α, ϕ_α) with local complex parameter z_α, $\omega = f_\alpha(z_\alpha)dz_\alpha$. Suppose two charts overlap $U_\alpha \cap U_\beta$, then

$$f_\beta(z_\beta) = f_\alpha(z_\alpha(z_\beta))\frac{dz_\alpha}{dz_\beta}.$$

If f_α is conformal for arbitrary local coordinates, then ω is called a *holomorhic 1-form*. All holomorphic 1-forms form a group, which is isomorphic to the first cohomology group of the surface. The holomorphic 1-form plays a crucial role in computing conformal mappings.

3.2 Quasi-Conformal Mapping

Suppose $(S_1, \mathcal{A}_1)$ and $(S_2, \mathcal{A}_2)$ are two Riemann surfaces and $\mathcal{A}_i$'s are their conformal structures. Suppose (U_α, ϕ_α) is a local chart of $\mathcal{A}_1$, and (V_β, ψ_β), is a local chart of $\mathcal{A}_2$. $\phi : S_1 \to S_2$ is a *conformal map* if and only if

$$\psi_\beta \circ \phi \circ \phi_\alpha^{-1} : \phi_\alpha(U_\alpha) \to \psi_\beta(V_\beta)$$

is biholomorphic. A conformal map preserves angles.

A generalization of the conformal map is called the *quasi-conformal* map which is an orientation-preserving homeomorphism between Riemann surfaces with bounded conformality distortion, in the sense that the first order approximation of the quasi-conformal homeomorphism takes small circles to small ellipses of bounded eccentricity. Thus, a conformal homeomorphism that maps a small circle to a small circle can also be regarded as quasi-conformal.

Mathematically, ϕ is quasi-conformal provided that it satisfies the Beltrami equation in Eqn. 1 on a local chart for some complex valued Lebesgue measurable μ satisfying $|\mu|_\infty < 1$. μ is called the *Beltrami coefficient*, which is a measure of conformality. In particular, the map ϕ is conformal around a small neighborhood of p when $\mu(p) = 0$. In general, ϕ maps an infinitesimal circle to a infinitesimal ellipse. From $\mu(p)$, we can determine the angles of the directions of maximal magnification as well as the amount of maximal magnification and maximal shrinking. Specifically, the angle of maximal magnification is $arg\mu(p)/2$ with magnifying factor $1 + |\mu(p)|$; the angle of maximal shrinking is the orthogonal angle $(arg\mu(p) - \pi)/2$ with shrinking factor $1 - |\mu(p)|$. The distortion or dilation is given by:

$$K = \frac{1 + |\mu(p)|}{1 - |\mu(p)|} \tag{2}$$

Thus, the Beltrami coefficient μ gives us all the information about the conformality of the map (See Fig. 2).

In terms of the metric tensor, considering the effect of the pullback under ϕ of the canonical Euclidean metric $\mathbf{g}_0$, the resulting metric is given by:

$$\phi^*(\mathbf{g}_0) = |\frac{\partial \phi}{\partial z}|^2 |dz + \mu(z)d\overline{z})|^2 \tag{3}$$

4 Computational Algorithm

This section introduces the computational algorithms for computing conformal mappings for surfaces based on holomorphic 1-form method.

4.1 Conformal Mapping

Doubly Connected Domain. Figure 4 shows a human face surface, with the mouth sliced open, therefore it is a doubly connected domain (a topological annulus). We denote the surface as S, its outer boundary as γ_1 and the inner boundary as γ_0, namely $\partial S = \gamma_1 - \gamma_0$. The conformal mapping $\phi : S \to \mathbb{C}$ is constructed as follows:

1. Compute a holomorphic 1-form ω, such that

$$Im(\int_{\gamma_1} \omega) = 2\pi,$$

where $Im()$ denotes the imaginary part.

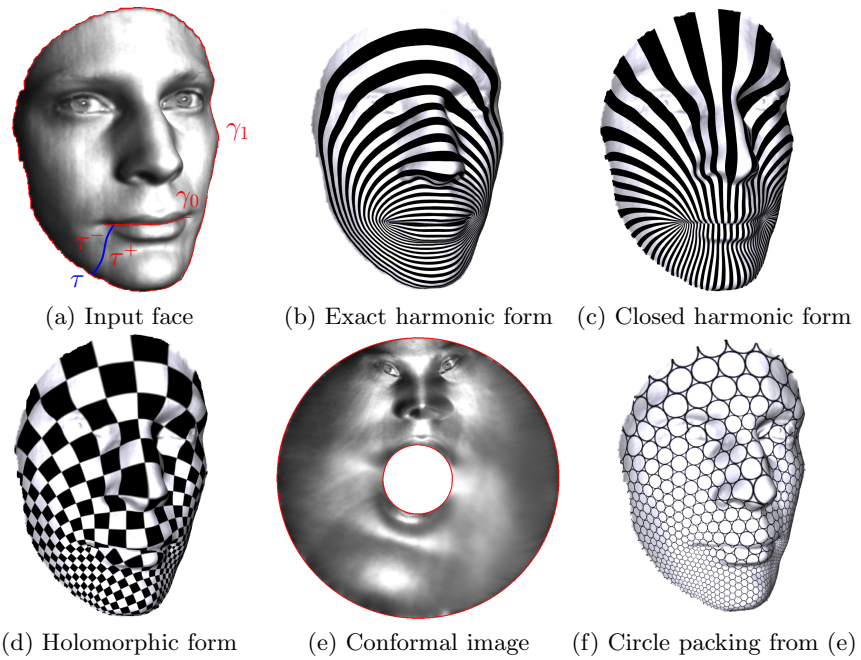

(a) Input face (b) Exact harmonic form (c) Closed harmonic form

(d) Holomorphic form (e) Conformal image (f) Circle packing from (e)

Fig. 4. Conformal mapping for doubly connected domain

2. Choose a base point $p \in S$, $Im(\phi(p)) = 0$. For any point $q \in S$, find an arbitrary path γ connecting p and q, then

$$\phi(q) = exp(\int_{\gamma} \omega).$$

We applied Gu-Yau's algorithm for computing the holomorphic 1-form, which is similar to that introduced in [11].

1. Compute a harmonic function $f : S \to \mathbb{R}$, such that

$$\begin{cases} \Delta f = 0 \\ f|_{\gamma_0} = 0 \\ f|_{\gamma_1} = 1 \end{cases}$$

   Let $\omega_1 = df$. Figure 4 (b) shows the exact harmonic 1-form ω_1.
2. Find a path τ connecting the two boundaries as shown in Fig. 4 (a). Slice the surface along the path to get a topological quadrilateral $\tilde{S}$, with boundaries $\gamma_0, \tau^+, \gamma_1, \tau^-$.
3. Randomly set a function $g : \tilde{S} \to \mathbb{R}$, such that

$$\begin{cases} g_{\tau^+} = 2\pi \\ g_{\tau^-} = 0 \end{cases}$$

   g is random on other points.
4. The gradient of g is a closed 1-form on S, denoted as $\tilde{\omega}_2 = dg$. Compute a function $h : S \to \mathbb{R}$, such that

$$\nabla \cdot (\tilde{\omega_2} + dh) = 0,$$

   with Neuman boundary condition

$$< \tilde{\omega}_2 + dh, \mathbf{n} >= 0,$$

   where $\mathbf{n}$ is the normal to the boundaries γ_0, γ_1. Let $\omega_2 = \tilde{\omega}_2 + dh$, Fig. 4 (c) shows the closed harmonic 1-form ω_2.
5. Find a constant c, such that

$$\int_{\tau} * \omega_2 = c \int_{\tau} \omega_1,$$

   where $*$ is the Hodge star operator. Then $\omega = c\omega_1 + \sqrt{-1}\omega_2$ is the desired holomorphic 1-form. Figure 4 (d) shows the holomorphic 1-form ω.

Simply Connected Domain. The construction of a conformal mapping for a simply connected domain (a topological disk) to the planar unit disk is very straight forward. Given a surface which is a topological disk, as shown in Fig. 1 (a), a small hole is punched at the point p. Then we map the punched disk, which is a topological annulus, to the planar annulus with the unit outer boundary. We choose a point q different from p, and map q to the real axis. We then shrink the size of the hole, and get another conformal mapping, still the outer boundary is with radius one, q is mapped to the real axis. If the size of the hole shrinks to zero, the conformal mapping of the annulus converges to the conformal mapping, such that p is mapped to the origin, q is mapped to the real axis. Figure 5 shows the conformal mapping result for a semi-cortex surface to the unit planar disk.

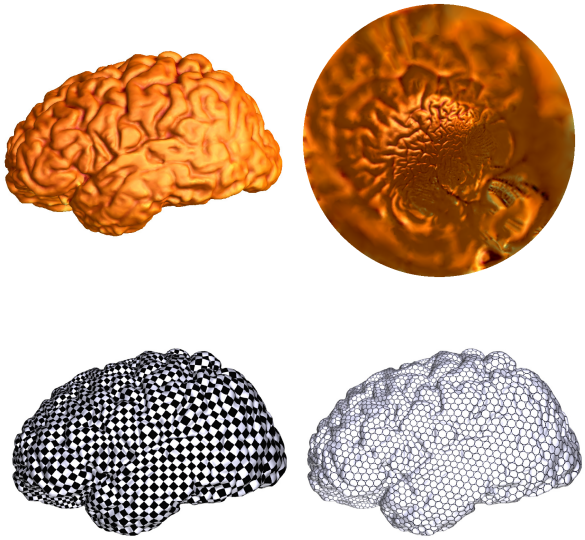

Fig. 5. Conformal mapping for simply connected domain

Multiply-Connected Domains. The construction of conformal mapping from a multiply connected domain to a planar disk with circular holes can be deduced to the doubly connected case by using Koebe's method [26]. As shown in Fig. 9, the human face surface in (a) is segmented to D_0, D_1, D_2, D_3, where D_0 is a multiply connected domain. The domain is conformally mapped to a planar disk with circular holes as shown in (b). The conformality is illustrated by texture mapping a circle packing pattern in (c), where all the small circles on the texture are mapped to circles on the surface.

The algorithm is as follows. The face surface is denoted as S. First, D_1 is removed from the surface S as shown in (d). Then the doubly connected domain $S - D_1$ is conformally mapped to a planar annulus as shown in (e). Then D_1 is glued back to the planar annulus by solving a harmonic map, such that the boundary of D_1 is mapped to the inner circle of the planar annulus. By using a scaling and a Möbius transformation, the conformal mapping is normalized, such that the point $p \in S$ is mapped to the origin, and the boundary point $q \in S$ is mapped to $+1$. The result is shown in (f). A similar procedure is repeated for segment D_2 shown in (g), (h) and (i), and for segment D_3 in (j), (k) and (l). By repeating this procedure, the images of the inner holes are getting rounder and rounder. Eventually, the images converge to a planar disk with circular holes where p is mapped to the origin, q is mapped to $+1$, as shown in (b).

The detailed proof for the convergence of Koebe's algorithm can be found in [26]. The convergence is very fast. In the example, the procedure only goes through each segment $D_k, k = 1, 2, 3$ once, and the images of the inner boundaries are very close to circles as shown in Fig. 9 (l).

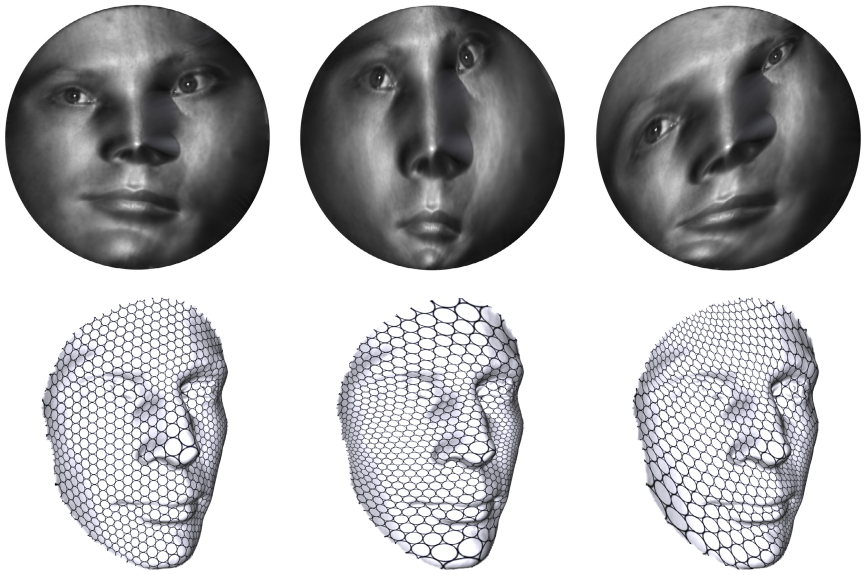

(a) $\mu = 0.0$ (b) $\mu = 0.25$ (c) $\mu = 0.25i$

Fig. 6. Quasi-Conformal mapping for a simply connected domain

4.2 Quasi-Conformal Maps

Simply Connected Domain. Given a surface S, which is a topological disk, two points $p, q \in S$, we want to compute a quasi-conformal map $\phi : S \to \mathbb{D}$, such that ϕ satisfies the Beltrami equation

$$\frac{\partial \phi}{\partial z} = \mu(z) \frac{\partial \phi}{\partial \overline{z}},$$

where z is the isothermal coordinate of S. Furthermore

$$\phi(p) = 0, \phi(q) \in \mathbb{R}^+.$$

First, we compute a conformal map $\phi_1 : S \to \mathbb{D}$, where $\mathbb{D}$ is the planar unit disk with the canonical Euclidean metric:

$$\mathbf{g}_0 = dz d\overline{z}.$$

Assume the Beltrami coefficient is defined on $\mathbb{D}$, $\mu : \mathbb{D} \to \mathbb{C}$, then we construct a new Riemannian metric $\mathbf{g}$ for $\mathbb{D}$,

$$\mathbf{g}(z) = |dz + \mu(z) d\overline{z}|^2. \tag{4}$$

We compute a conformal map $\phi_2 : (\mathbb{D}, \mathbf{g}) \to (\mathbb{D}, \mathbf{g}_0)$, such that $\phi_2(\phi_1(p)) = 0, \phi_2(\phi_1(q)) \in \mathbb{R}^+$. Then the quasi-conformal map is given by $\phi = \phi_2 \circ \phi_1$, $\phi : S \to (\mathbb{D}, \mathbf{g}_0)$, which satisfies the Beltrami equation.

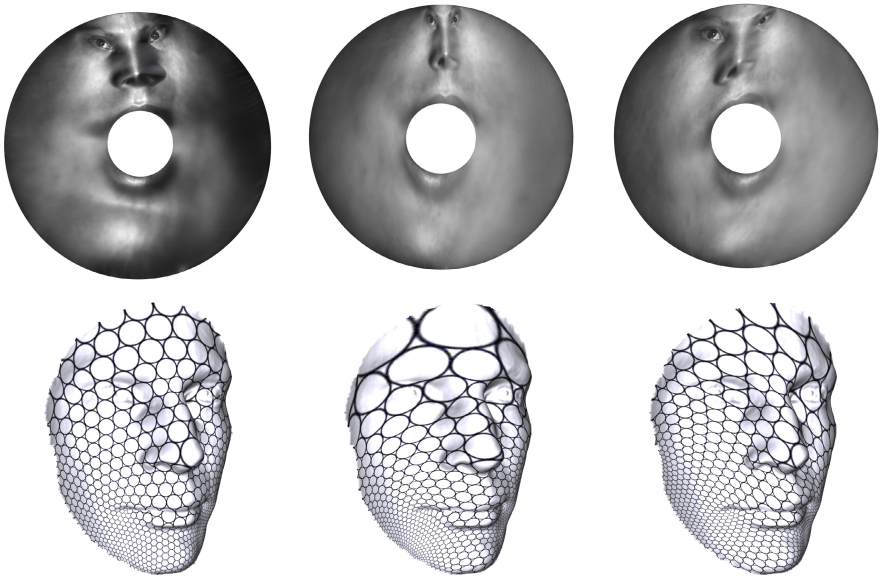

(a) $\mu = 0.0$ (b) $\mu = 0.25$ (c) $\mu = 0.25i$

Fig. 7. Quasi-Conformal mapping for a doubly connected domain

Doubly Connected Domain. Similarly, if S is a topological annulus, first a conformal map $\phi_1 : S \to A^2$ is computed using the algorithm discussed above, where A^2 is a planar annulus with canonical Euclidean metric $\mathbf{g}_0$, whose boundaries are concentric circles. Similarly, a new metric $\mathbf{g}$ is constructed for T^2 using Formula 4. Then a conformal map $\phi_2 : (A^2, \mathbf{g}) \to (\tilde{A}^2, \mathbf{g}_0)$ is computed, where $\tilde{A}^2$ is another planar annulus with canonical Euclidean metric and concentric boundary circles. The shape of $\tilde{A}^2$ is determined automatically by $(T^2, \mathbf{g})$. The quasi-conformal map ϕ is given by the composition of ϕ_1 and ϕ_2, $\phi : \phi_2 \circ \phi_1 : S \to (\tilde{A}^2, \mathbf{g}_0)$.

Multiply Connected Domain. Suppose S is a multiply connected domain with boundaries

$$\partial S = \gamma_0 - \gamma_1 - \cdots - \gamma_n$$

First, we fill all the holes with topological disks $D_1, D_2, \cdots D_n$, such that $\partial D_k = \gamma_k$. Then $\tilde{S} = S \cup \{\bigcup_k D_k\}$ is a simply connected domain. Then we compute a conformal map $\phi_1 : \tilde{S} \to \mathbb{D}$. We can extend the Beltrami coefficient μ to $\tilde{\mu}$ on $\mathbb{D}$ from $\phi_1(S)$ to $\phi_1(D_k)$'s by solving harmonic functions using Dirichlet boundary condition,

$$\tilde{\mu}(p) = \mu(p), \forall p \in S; \Delta\tilde{\mu}(p) = 0, p \in \bigcup_k D_k.$$

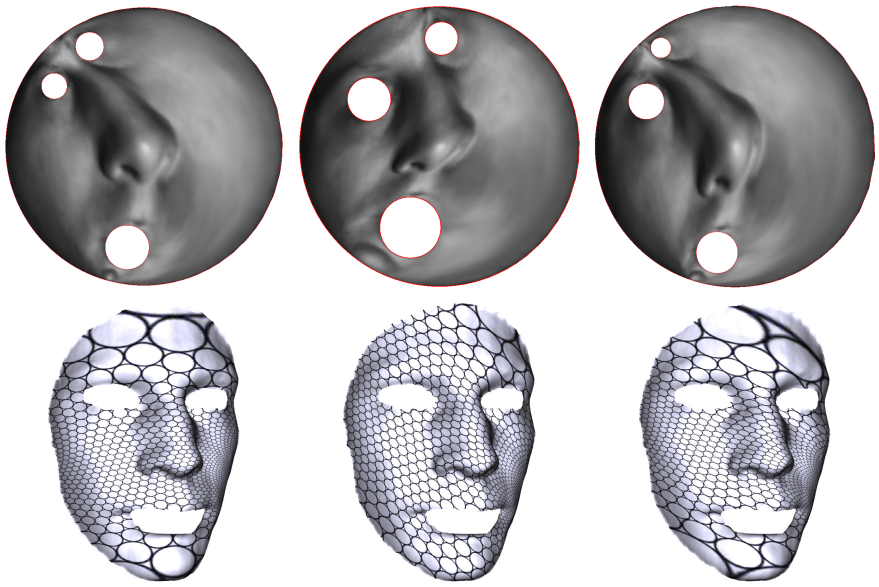

(a) $\mu = 0.25$ (b) $\mu = 0.25i$ (c) $\mu = 0.25 + 0.25i$

Fig. 8. Quasi-Conformal mapping for a multiply connected domain

Then we can compute a quasi-conformal map $\phi_2 : (\mathbb{D}, \mathbf{g}_0) \to (\mathbb{D}, \mathbf{g}_0)$, such that

$$\frac{\partial \phi_2}{\partial \bar{z}} = \tilde{\mu}(z) \frac{\partial \phi_2}{\partial z}$$

Then we can compute a conformal map from a planar multiply connected domain $(\phi_2 \circ \phi_1(S), \mathbf{g}_0)$ with canonical Euclidean metric to a planar disk with circular holes, $\phi_3 : \phi_2 \circ \phi_1(S) \to (\mathbb{D}, \mathbf{g}_0)$. The desired quasi-conformal map ϕ is the composition

$$\phi = \phi_3 \circ \phi_2 \circ \phi_1 : S \to (\mathbb{D}, \mathbf{g}_0),$$

which satisfies the Beltrami equation (see Eqn. 1).

4.3 Discrete Algorithm

In practice, all the surfaces are approximated by simplicial-complexes embedded in $\mathbb{R}^3$, denoted as $M = (V, E, F)$, where V, E, F are the sets of vertices, edges and faces respectively. We use v_i to denote the i-th vertex, $[v_i, v_j]$ the halfedge from v_i to v_j, $[v_i, v_j, v_k]$ the face with vertices v_i, v_j, v_k, sorted counter clockwisely. A discrete 0-form $f : V \to \mathbb{R}$ is a real valued function defined on the vertices. A discrete 1-form $\omega : E \to \mathbb{R}$, defined on edges. The exterior differentiation operator is defined as

$$df([v_i, v_j]) = f(v_j) - f(v_i).$$

and

$$d\omega([v_i, v_j, v_k]) = \omega([v_i, v_j]) + \omega([v_j, v_k]) + \omega([v_k, v_i]).$$

ω is a closed 1-form, if $d\omega = 0$.

Suppose two faces $[v_i, v_j, v_k]$ and $[v_j, v_i, v_l]$ share an edge $[v_i, v_j]$. The weight on edge $[v_i, v_j]$ is defined as

$$w_{ij} = \cot \theta_k^{ij} + \cot \theta_l^{ij},$$

where θ_k^{ij} is the corner angle at the vertex v_k in the face $[v_i, v_j, v_k]$: θ_l^{ij} is defined in the similar way. If the edge $[v_i, v_j]$ is on the boundary and only attached to $[v_i, v_j, v_k]$ then the edge weight is defined as

$$w_{ij} = \cot \theta_k^{ij}.$$

The discrete harmonic energy of a 0-form $f : V \to \mathbb{R}$ is defined as

$$E(f) = \sum_{[v_i, v_j]} w_{ij}(f(v_j) - f(v_i))^2.$$

The *divergence operator* is defined as

$$\nabla \cdot \omega(v_j) = \sum_j w_{ij}\omega([v_i, v_j]),$$

where v_j are all the vertices connecting to v_i. A discrete harmonic 1-form satisfies $\nabla \cdot \omega = 0$.

Let ω be a closed 1-form. A face $[v_i, v_j, v_k]$ can be isometrically embedded on the plane, and then ω has local representation as $\omega = adx + bdy$. The *Hodge star operator* is defined as ${}^*\omega = -bdx + ady$, where a, b are two real numbers and the *wedge product* between two closed 1-forms $\omega_k = a_k dx + b_k dy,\ k = 1, 2$ is given by

$$\omega_1 \wedge \omega_2 = \begin{vmatrix} a_1 & b_1 \\ a_2 & b_2 \end{vmatrix} dx \wedge dy \tag{5}$$

The inner product between ω_1 and ω_2 is defined as

$$< \omega_1, \omega_2 >= \int_M \omega_1 \wedge {}^*\omega_2. \tag{6}$$

Let M be a triangular mesh of genus g. We first compute its first homology group $H_1(M, \mathbb{Z})$ basis by CW-cell decomposition, which we denote by $\{\gamma_1, \gamma_2, \cdots, \gamma_{2g}\}$. Then we compute the dual basis for the cohomology group $H^1(M, \mathbb{R})$, $\{\tau_1, \tau_2, \cdots, \tau_{2g}\}$, such that

$$\int_{\gamma_i} \tau_j = \delta_{ij}.$$

Then we find 0-forms $g_i : M \to \mathbb{R}$, such that

$$\nabla \cdot (\tau_i + dg_i) = 0, i = 1, 2, \cdots, 2g,$$

then $\omega_i = \tau_i + dg_i$'s are harmonic 1-forms. The Hodge star of a harmonic 1-form is also harmonic, therefore

$$^*\omega_i = \sum_j \lambda_{ij}\omega_j,$$

the coefficient of λ_{ij} can be computed by solving the linear system

$$< \omega_k, \omega_i >= \sum_j \lambda_{ij} \int_M \omega_k \wedge \omega_j, k = 1, 2, \cdots, 2g,$$

the left hand side is computed using formula 6, the right hand side by Formula 5. The holomorphic 1-form basis is given by

$$\{\omega_1 + \sqrt{-1}^*\omega_1, \omega_2 + \sqrt{-1}^*\omega_2, \cdots, \omega_{2g} + \sqrt{-1}^*\omega_{2g}\}.$$

Surfaces with boundaries can be converted to symmetric closed surfaces by double covering and therefore their holomorphic 1-form group basis can be computed in the similar way. For details, we refer readers to Gu and Yau's work [11]. Conformal mappings between genus zero surfaces with boundaries can be carried out using holomorphic 1-forms, which can be approximated in the discrete setting.

By the above discrete forms and the operators, the algorithms described in previous two subsections can be carried out in the discrete setting.

5 Experimental Results

Most of the surfaces are captured using 3D scanner based on phase shifting principle [27, 28]. The scanned resolution is 640×480, at 60 frames per second. The triangulations are directly determined by the pixel grid structure of the scanned images. We did not perform preprocessing operations, such as smoothing, denoising and mesh simplification. The raw data sets are computed using the algorithms described above. This demonstrates the robustness of our method.

All the algorithms are implemented using generic C++ on a Windows XP platform with Dual 2.33GHz CPU and 3.98 GB of RAM. The linear systems are in general symmetric and positive definite. We use the Matlab C++ library as the linear solver.

In our experiment, the surfaces are described as triangular meshes. The Beltrami coefficient μ is a function over the whole surface. In Fig. 1(e), the μ is set to be $x + iy$ for each vertex. The quasi-conformal mappings are constructed using holomorphic differential forms, which is general for surfaces with different topologies. In other cases, it is set to be a constant complex number. Table 1 lists the computational time for each case with different Beltrami coefficient μ. For large meshes with $160k$ faces, the processing time for Koebe's method [26] with multiple iterations is about 2.5 minutes. This demonstrates the efficiency of our algorithm.

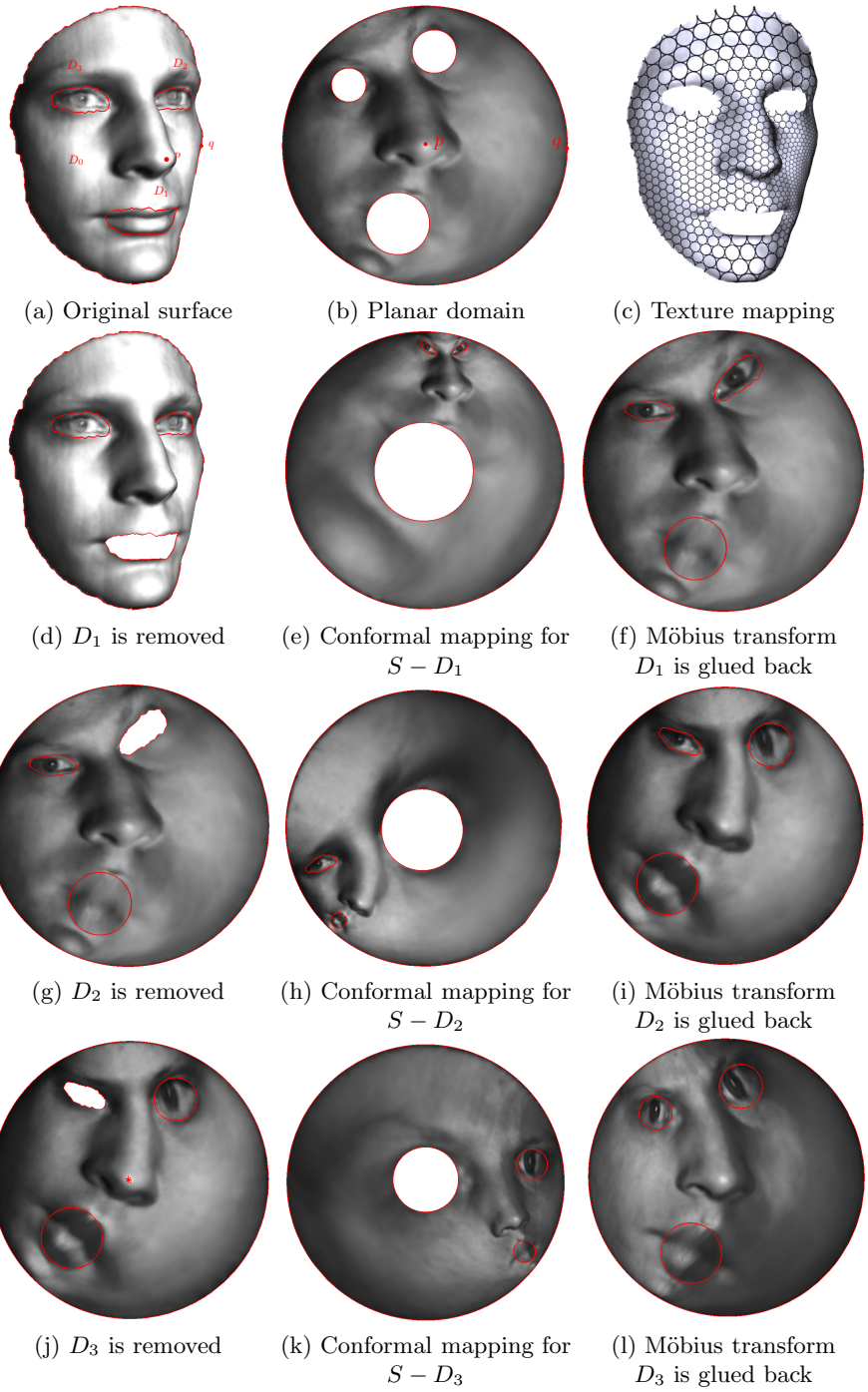

(a) Original surface (b) Planar domain (c) Texture mapping

(d) D_1 is removed (e) Conformal mapping for $S - D_1$ (f) Möbius transform D_1 is glued back

(g) D_2 is removed (h) Conformal mapping for $S - D_2$ (i) Möbius transform D_2 is glued back

(j) D_3 is removed (k) Conformal mapping for $S - D_3$ (l) Möbius transform D_3 is glued back

Fig. 9. Conformal mapping for a multiply connected domain using Koebe's algorithm

Table 1. Computational Time

Figure	#Vertex	#Face	#Boundary	Beltrami Coefficient μ	Iterations	Time
Fig. 1(e)	80593	160054	1	$x + iy$	1	102s
Fig. 6(a)	80593	160054	1	$0.00 + 0.00i$	1	73s
Fig. 6(b)	80593	160054	1	$0.25 + 0.00i$	1	110s
Fig. 6(c)	80593	160054	1	$0.00 + 0.25i$	1	105s
Fig. 7(a)	80724	160054	2	$0.00 + 0.00i$	1	78s
Fig. 7(b)	80724	160054	2	$0.25 + 0.00i$	1	110s
Fig. 7(c)	80724	160054	2	$0.00 + 0.25i$	1	112s
Fig. 9(c)	15160	29974	4	$0.00 + 0.0i$	2	156s
Fig. 8(a)	15160	29974	4	$0.25 + 0.0i$	2	160s
Fig. 8(b)	15160	29974	4	$0.00 + 0.25i$	2	156s
Fig. 8(c)	15160	29974	4	$0.25 + 0.25i$	2	157s

Besides the scanned data sets, we also test human cortex surface as shown in Fig. 5. The surface is reconstructed from MRI images. Furthermore, we tested some synthetic data to verify the accuracy of our method. The algorithm recovers the correct solution with high accuracy.

6 Conclusion and Future Works

This work introduces a rigorous method for computing quasi-conformal mappings by solving Beltrami equations. The method is efficient and robust. The major point is to deform the Riemannian metric by the Beltrami coefficient and convert a quasi-conformal mapping to a conformal mapping. In the current work, the method is based on holomorphic differentials, and it can be directly generalized to discrete Ricci flow [29,3,4] and to the Yamabe flow method [30,31,32].

In the future, we plan to apply quasi-conformal mappings to shape registration, surface comparison, shape recognition, and many other applications in computer graphics, computer vision, medical imaging and geometric modeling. Also, we will explore rigorous algorithms for computing extremal quasi-conformal maps.

Acknowledgement

The authors would like to thank Prof. Ralph Martin, Prof.Arie Kaufman and Prof. Hong Qin for the discussion. This work is partially supported by NSF 0448399 career: Conformal Geometry Applied to Shape Analysis and Geometric Modeling and NSF 0626223: Discrete Curvature Flow.

References

1. Floater, M.S., Hormann, K.: Surface parameterization: a tutorial and survey. In: Advances in Multiresolution for Geometric Modelling, pp. 157–186. Springer, Heidelberg (2005)

2. Kraevoy, V., Sheffer, A.: Cross-parameterization and compatible remeshing of 3d models. ACM Transactions on Graphics 23(3), 861–869 (2004)
3. Jin, M., Kim, J., Gu, X.D.: Discrete surface ricci flow: Theory and applications. In: Martin, R., Sabin, M.A., Winkler, J.R. (eds.) Mathematics of Surfaces 2007. LNCS, vol. 4647, pp. 209–232. Springer, Heidelberg (2007)
4. Jin, M., Kim, J., Luo, F., Gu, X.: Discrete surface ricci flow. IEEE Transaction on Visualization and Computer Graphics 14(5), 1030–1043 (2008)
5. Pinkall, U., Polthier, K.: Computing discrete minimal surfaces and their conjugates. Experimental Mathematics 2(1), 15–36 (1993)
6. Lévy, B., Petitjean, S., Ray, N., Maillot, J.: Least squares conformal maps for automatic texture atlas generation. In: SIGGRAPH 2002, pp. 362–371 (2002)
7. Desbrun, M., Meyer, M., Alliez, P.: Intrinsic parameterizations of surface meshes. Computer Graphics Forum (Proc. Eurographics 2002) 21(3), 209–218 (2002)
8. Floater, M.S.: Mean value coordinates. Computer Aided Geometric Design 20(1), 19–27 (2003)
9. Gotsman, C., Gu, X., Sheffer, A.: Fundamentals of spherical parameterization for 3D meshes. ACM Transactions on Graphics 22(3), 358–363 (2003)
10. Gu, X., Wang, Y., Chan, T.F., Thompson, P.M., Yau, S.-T.: Genus zero surface conformal mapping and its application to brain surface mapping. IEEE Trans. Med. Imaging 23(8), 949–958 (2004)
11. Gu, X., Yau, S.-T.: Global conformal parameterization. In: Symposium on Geometry Processing, pp. 127–137 (2003)
12. Mercat, C.: Discrete riemann surfaces and the ising model. Communications in Mathematical Physics 218(1), 177–216 (2004)
13. Hirani, A.N.: Discrete exterior calculus. PhD thesis, California Institute of Technology (2003)
14. Jin, M., Wang, Y., Yau, S.-T., Gu, X.: Optimal global conformal surface parameterization. In: IEEE Visualization 2004, pp. 267–274 (2004)
15. Gortler, S.J., Gotsman, C., Thurston, D.: Discrete one-forms on meshes and applications to 3D mesh parameterization. Computer Aided Geometric Design 23(2), 83–112 (2005)
16. Tong, Y., Alliez, P., Cohen-Steiner, D., Desbrun, M.: Designing quadrangulations with discrete harmonic forms. In: Symposium on Geometry Processing, pp. 201–210 (2006)
17. Tewari, G., Gotsman, C., Gortler, S.J.: Meshing genus-1 point clouds using discrete one-forms. Comput. Graph. 30(6), 917–926 (2006)
18. Desbrun, M.: Discrete differential forms and applications to surface tiling. In: SCG 2006: Proceedings of the twenty-second annual symposium on Computational geometry, p. 40. ACM, New York (2006)
19. Tong, Y., Alliez, P., Cohen-Steiner, D., Desbrun, M.: Designing quadrangulations with discrete harmonic forms. In: SGP 2006: Proceedings of the fourth Eurographics symposium on Geometry processing, pp. 201–210 (2006)
20. Hong, W., Gu, X., Qiu, F., Jin, M., Kaufman, A.E.: Conformal virtual colon flattening. In: Symposium on Solid and Physical Modeling, pp. 85–93 (2006)
21. Wang, S., Wang, Y., Jin, M., Gu, X.D., Samaras, D.: Conformal geometry and its applications on 3d shape matching, recognition, and stitching. IEEE Trans. Pattern Anal. Mach. Intell. 29(7), 1209–1220 (2007)
22. Zeng, W., Zeng, Y., Wang, Y., Yin, X., Gu, X., Samaras, D.: 3d non-rigid surface matching and registration based on holomorphic differentials. In: Forsyth, D., Torr, P., Zisserman, A. (eds.) ECCV 2008, Part III. LNCS, vol. 5304, pp. 1–14. Springer, Heidelberg (2008)

23. Gu, X., He, Y., Qin, H.: Manifold splines. Graphical Models 68(3), 237–254 (2006)
24. Guggenheimer, H.W.: Differential Geometry. Dover Publications (1977)
25. Farkas, H.M., Kra, I.: Riemann Surfaces. Springer, Heidelberg (2004)
26. Henrici, P.: Applide and Computational Complex Analysis, Discrete Fourier Analysis, Cauchy Integrals, Construction of Conformal Maps, Univalent Functions, vol. 3. Wiley-Interscience, Hoboken (1993)
27. Wang, Y., Gupta, M., Zhang, S., Samaras, D., Huang, P.: High resolution tracking of non-rigid 3D motion of densely sampled data using harmonic maps. In: Proc. International Conference on Computer Vision, pp. 388–395 (2005)
28. Gu, X., Zhang, S., Huang, P., Zhang, L., Yau, S.-T., Martin, R.: Holoimages. In: SPM 2006: Proceedings of the 2006 ACM symposium on Solid and physical modeling, pp. 129–138 (2006)
29. Chow, B., Luo, F.: Combinatorial ricci flows on surfaces. Journal Differential Geometry 63(1), 97–129 (2003)
30. Luo, F.: Combinatorial yamabe flow on surfaces. Commun. Contemp. Math. 6(5), 765–780 (2004)
31. Springborn, B., Schröder, P., Pinkall, U.: Conformal equivalence of triangle meshes. ACM Trans. Graph. 27(3), 1–11 (2008)
32. Zeng, W., Jin, M., Luo, F., Gu, X.: Computing canonical homotopy class representative using hyperbolic structure. In: IEEE International Conference on Shape Modeling and Applications (SMI 2009) (2009)